DOI 10.4430/bgo00418

Moho relief modelling by gravity data using the Maximum Difference Reduction method: the case of central Zagros, Iran

M. Khaleghi Yalehgonbadi and V.E. Ardestani

Institute of Geophysics, University of Tehran, Tehran, Iran

(Received: 21 February 2023; accepted: 28 May 2023; published online: 16 February 2024)

ABSTRACT We have conducted a gravity study using ground gravity data, via an automated iterative forward modelling method, to determine the Moho depth map in parts of the Zagros Mountains. The method used, the Maximum Difference Reduction (MDR) method, consists in a modification of the well-known Bott method for solving nonlinear inverse problems. The main characteristics of the MDR algorithm are: 1) the subsurface is divided into rectangular blocks to determine the gravity effect; 2) the density contrast is defined as *a priori* information, and is considered constant in the whole body. Therefore, we have no non-uniqueness; 3) depth correction in any station stops when the sign of a residual gravity anomaly differs from that of an observed one. As a result, the algorithm moves in one direction, and convergence occurs; 4) the inversion process stops when the residual anomalies fall within a predefined error range, which is controlled by the chi-square criteria. The method has been examined through a synthetic model and, then, applied to determine the Moho depth under the Zagros Mountains. The maximum Moho depth in the Zagros fold-thrust belt, Sanandaj-Sirjan zone, Urumieh-Dokhtar magmatic arc and central Iran, are found respectively at 45, 68, 52, and 42 km.

Key words: Zagros belt, Moho depth, gravity data, maximum difference reduction, iterative method, 2D nonlinear inversion.

1. Introduction

The Moho (or the Mohorovičić) discontinuity is the boundary between the lowermost crust and the underlying mantle in the Earth. It is between 25 and 80 km deep beneath the continents, and 5 and 20 km deep beneath the ocean floor. This boundary is characterised by the distinct change in the velocity of seismic waves and by an intense increase in density. Therefore, its depth is usually estimated by seismological or gravimetric methods.

The Zagros Mountain belt is an active and young orogen created by the convergence of the Arabia-Eurasia plate during the Mesozoic and Cenozoic period (Berberian and King, 1981; Berberian *et al*., 1982; Mouthereau *et al*., 2012). Such belt is substantial for the geoscientific community as it is a well-exposed case of a continent-continent collision belt at an early stage of its evolution. Therefore, estimating crustal thickness underneath the Zagros Mountains can give key constraints on the lithospheric structure, for a better understanding of the dynamics of this mountain range, which has been studied, using different geophysical methods, by many researchers.

Dehghani and Makris (1984) obtained the crustal thickness variations in Iran through Bouguer anomaly modelling and suggested Moho depths of 50-55 km underneath central

Zagros, and 40-45 km in central Iran. Snyder and Barazangi (1986) did the same for Zagros and estimated a maximum Moho depth of 65 km in this region. Molinaro *et al*. (2005) presented a balanced cross-section of the south-eastern Zagros Fold-Thrust Belt (ZFTB) and found a 52-kilometre Moho depth in central Zagros. Paul *et al*. (2006) used temporary seismological stations across central Zagros, computed crustal receiver functions, and obtained Moho depths of 70 km underneath the Sanandaj-Sirjan Zone (SSZ), and 42 km in central Iran. Manaman and Shomali (2010) imaged Moho depth variations across the Zagros collisional zone via the Partitioned Waveform Inversion (PWI) method. They estimated the Moho depth to be about 40-45 km throughout their profile with abrupt crustal thickening in the middle up to about 65 km. Manaman *et al*. (2011), through the PWI method, and applying *a priori* knowledge, estimated a Moho depth of 45 km beneath the ZFTB, with a maximum of 65 km under the Main Zagros Thrust (MZT), and the SSZ, and ~42 km below the Urumieh-Dokhtar Magmatic Arc (UDMA) and southern part of central Iran. Paul *et al*. (2010) presented a high-resolution image of the Moho beneath seismic transects obtained by receiver function analysis of teleseismic earthquake records. They found an average crust thickness of 43±2 km beneath the ZFTB and the central domain. Motavalli-Anbaran *et al*. (2011) modelled the crustal thickness by combining different potential field data sets and found 60 km underneath MZT and 38-39 km in central Iran. Jiménez-Munt *et al*. (2012) proposed a first-order estimate of the crustal thickness by calculating the geoid height and elevation data combined with the thermal analysis, and computed the Moho depth below the high Zagros at ~60 km. Motaghi *et al*. (2015) obtained the structure of Iran, beneath a seismic profile, by simultaneously inverting data from receiver functions and fundamental-mode Rayleigh wave group velocity. They confirmed their results by modelling Bouguer gravity anomaly data; Moho depths of ~50 km beneath Zagros, ~59 km beneath the SSZ and UDMA, and ~35 km beneath central Iran were found. Tunini *et al*. (2015) applied a combined geophysical-petrological method and acquired minimum values beneath central Iran (42-43 km), and maximum values beneath the SSZ (55-63 km). Mousavi and Ebbing (2018) estimated the crustal structural domains beneath the Iranian plateau by inversion of elevation and geoid anomaly data combined with thermal analysis. They found Moho depths of 30 to 60 km. Mousavi and Fullea (2020) modelled the crustal structure of the Iranian plateau by integrated geophysical-petrological modelling. Their results indicate that the deepest Moho boundary is located beneath the high Zagros Mountains (~65 km).

In all methods mentioned above, determining depth with geophysical methods is a nonlinear problem that can be solved through the iteration or approximation of a problem from nonlinear to linear (Blakely 1996).

The main challenge in using geophysical methods, especially in gravimetry, is that the responses in these procedures suffer from extreme non-uniqueness and instability. Non-uniqueness in gravimetric methods occurs for two reasons: theoretical and algebraic ambiguity. Theoretical ambiguity is due to the nature of gravity. Many equivalent sources in the subsurface can produce the same data at the surface (Jackson, 1979). Algebraic ambiguity occurs when the parameterisation of the problem creates an underdetermined situation with more unknowns than observations. Ill-conditioned kernel matrices and data noise are also important causes of instability in gravimetric methods. For these reasons, we are exposed to an ill-posed problem (Blakely, 1996; Freeden, 2021).

Tikhonov regularisations are common to remove ill-posed problems (Hansen, 1998; Vogel, 2002). It is also possible to insert *a priori* information (obtained from geological studies or theoretical estimates) and constraints into the algorithm and fix the ill-posed part of the problem

in an iterative process (Bott, 1960; Parker, 1973; Oldenburg, 1974; Pilkington and Crossley, 1986; Leão *et al*., 1996; Barbosa *et al*., 1997, 1999a, 1999b).

In the light of the aforementioned, to improve the knowledge on orogenic processes, in this paper, we intend to study crustal thickness variations across the Zagros Mountains via the Maximum Difference Reduction (MDR) algorithm. This algorithm has already been used to find the thickness of shallow sedimentary basins (Zhou, 2013). We used ground gravity data in the inversion process. These data are the densest and most accurate data set available. The MDR algorithm does not require the addition of many constraints or user intervention, and provides us with an automatic interpretation of the geophysical data. To overcome ill-posedness and non-linearity, this method applies conditions and constraints in an iterative process to guarantee the stability and convergence of the algorithm. The results of synthetic models, and previous geophysical studies conducted in this area, can be an excellent basis to examine inversion algorithm responses. After a brief description of the geology and data available, we will present the method, apply it to a synthetic model and to central Zagros, and, then, illustrate its transition to the Iranian plateau as a real case.

2. Geological settings

The study area includes parts of the Zagros orogenic belt and central Iran. We modelled three 2D profiles in the SW-NE direction across the ZFTB, SSZ, UDMA, and NW of central Iran; and the tectonic characteristics of these areas are reviewed as follows (Fig. 1).

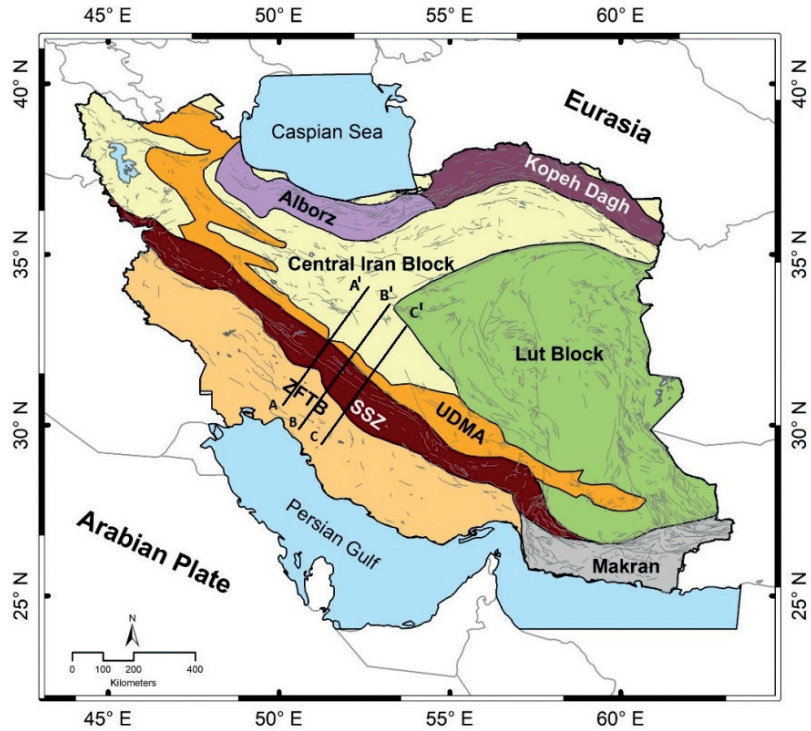

Fig. 1 - Simplified regional geological map of Iran including the Zagros Fold-Thrust Belt (ZFTB), Sanandaj-Sirjan Zone (SSZ), Urumieh-Dokhtar Magmatic Arc (UDMA), and other structural units along with three profiles (AA', BB', and CC').

The Zagros orogenic belt of Iran, as part of the Alpine-Himalayan mountain chain, extends for about 2,000 km in a NW-SE direction, from the East Anatolian Fault of eastern Turkey to the Oman line in southern Iran (Alavi, 1994). This orogeny has undergone three successive geological events. The first occurred during the Early to Late Cretaceous, and included the subduction of the Neo-Tethyan oceanic plate beneath the Iranian lithosphere. The second occurred in the Late Cretaceous, and consisted in the obduction of Neo-Tethyan oceanic ophiolites over the Afro-Arabian passive continental margin. The third event consists in the collision of the Afro-Arabian continental lithosphere with the Iranian plate, which started during the Late Cretaceous (Alavi, 1994).

From NE to SW (Fig. 1), the Zagros orogeny comprises three parallel belts: the UDMA, SSZ, and ZFTB.

The UDMA, with a width of 50 km, is composed of intrusive and extrusive rocks of the Eocene-Quaternary age (Berberian and King, 1981), produced by the collision of the Arabian and central Iranian continental plate margins. Magmatic activity and north-eastward thrust faulting in this region are the results of the increased thickness of the continental crust (Alavi, 1994).

The SSZ, with a length of about 1,500 km in Iran, was shaped by tectonic processes such as folding and metamorphosis during the Early Cimmerian orogeny, tectonisation in the Upper Cretaceous, and deformation (along the ZMT). The outer belt of imbricate thrust slices and the inner belt, mainly of Mesozoic metamorphic rocks, form the SSZ. In this zone, metamorphic rocks are observed with large deformed and undeformed plutons (Berberian, 1997).

The ZFTB forms the less strained external part of the Zagros orogeny, and consists of a pile of folded and faulted rocks made up of 4 to 7 km of mainly Palaeozoic and Mesozoic successions, overlain by 3 to 5 km of Cenozoic siliciclastic and carbonate rocks. This belt, which lies on a highly metamorphosed Proterozoic Pan-African basement, was affected by the late Neoproterozoic–Cambrian Najd strike-slip faults (Brown and Jackson, 1960; Agar, 1987; Husseini, 1988). The south-western boundary of the ZFTB defines the current Zagros Deformational Front (ZDF), to the SW of which deformation has not yet propagated.

The central Iranian zone is known as a triangular area. It is located between the Alborz and Kopeh Dagh range to the north, and the Zagros and Makran range to the west and south. The central Iranian crust, before becoming part of Eurasia (after the opening of the Neotethys in the Triassic), was decoupled as part of Africa. This microplate, formed in pre-Palaeozoic, shows no indication of Variscan orogeny (Delaloye *et al*., 1981). It is fragmented into several blocks by crustal faults (the Great Kavir, Nain-Baft, and Harirud faults). From east to west, these blocks are the Lut Block, the Tabas Block, and the Yazd Block (Berberian *et al*., 1982). These blocks detached from Gondwana in the late Palaeozoic and accreted to Eurasia in the Mesozoic, inducing Cimmerian collisional events (Zanchi *et al*., 2009a, 2009b). In contrast to the surrounding areas, the western part of central Iran is covered by currently subsiding basins. It is highly aseismic and, therefore, considered to behave as a rigid block (Jackson *et al*., 1995; Allen *et al*., 2004; Guest *et al*., 2007).

3. Data

The Bouguer anomaly data used in this paper have been acquired by the National Cartographic Center (NCC) of Iran. These grid data are of the terrestrial data type, and are the best in terms of accuracy and completeness. The Bouguer anomaly values range between -80 mGal at the south-western ZFTB, and -218 mGal in some parts of the SSZ. The data precision is about 5 μGal. In addition, the distance between points on the grid is between 5 and 10 km. Topography

data were provided from 1 min TOPEX global data sets (ftp://topex.ucsd. edu/pub). A complete Bouguer anomaly map was obtained after applying terrain correction to the data with a radius of 100 km, and taking 2,670 kg/m^3 as the average terrain density in the area. The survey area is in the Zagros Mountains region. Since our research is two-dimensional, we selected three profiles crossing the area, roughly in the SW-NE direction from this grid. The Bouguer anomaly map and the three selective profiles are shown in Fig. 2.

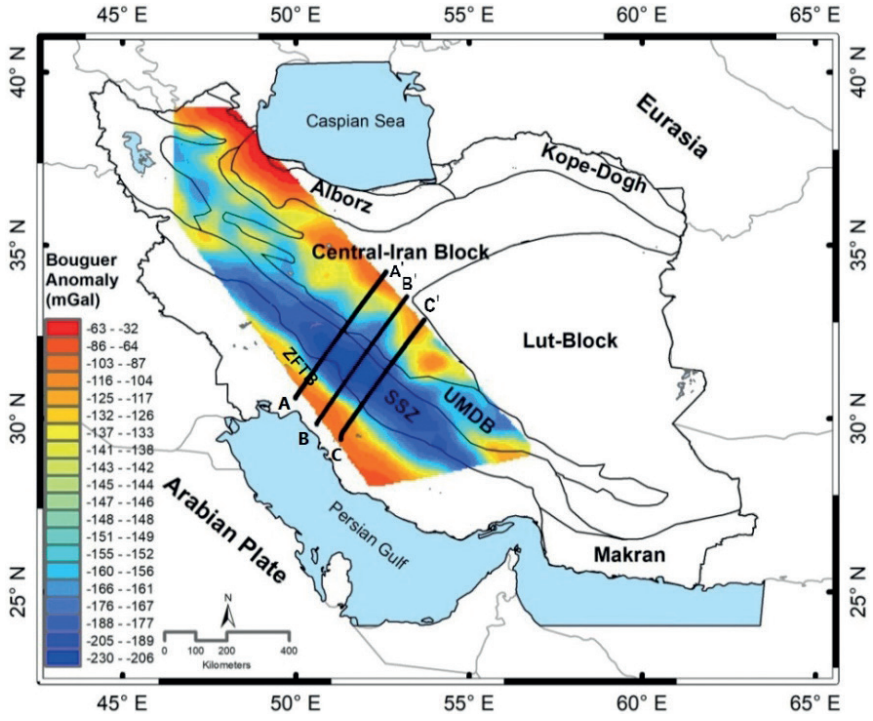

Fig. 2 - Bouguer gravity anomalies of Zagros from ground gravity data prepared by the NCC of Iran. Three profiles, AA', BB', and CC', are used in inversion modelling.

4. Gravity modelling

4.1. Forward modelling

The relationship between surface-observed gravity data and subsurface density is defined in a forward equation. The vertical component of the gravitational attraction of a two-dimensional body, at the origin using the Cartesian coordinate system, is given by (Blakely, 1996):

$$g_i = 2\gamma\rho \int_z \int_x \frac{zdxdz}{x^2 + z^2}. \quad (1)$$

Here γ is the universal gravitational constant, ρ is the density and assumed constant within the body, and x and z are the distances from one point in the body to the origin. A numerical solution of this integral, for an L-sided polygon, is given by (Blakely, 1996):

$$g_i = 2\gamma\rho \sum_{p=1}^{l} \frac{v_p}{1+\psi_p^2}\left[log\frac{r_{p+1}}{r_p} - \psi_p(\theta_{p+1} - \theta_p)\right] \quad (2)$$

where

$$\psi_p = \frac{x_{p+1} - x_p}{z_{p+1} - z_p}$$

and

$$v_p = x_p - \psi_p z_p$$

where r is the distance of the polygon vertices from the origin, θ is the r angle with positive direction of the x-axis, and p is the number of sides of the polygon.

In this study, we used a set of juxtaposition rectangular blocks (p = 4), extended downwards and parallel to the vertical axis, with different depth limits for simulating underground structures (Fig. 2). Fig. 2 shows the discretisation of sediment layers using 2D prisms. The grey prisms represent the sediment layer, while the white prisms correspond to the basement. The top of each prism is fixed according to the topography, while their bottom depths are to be estimated in the inversion process. The plus signs on the top centre of the prisms indicate the observation points on the surface.

The term on the right-hand side of Eq. 2 quantifies the contribution to the i-th data point of a unit density in the j-th cell (G_{ij}). This response is valid only at station and for one prism. To obtain the total response at each i station, the gravity responses of N prisms are summed:

$$g_i = \sum_{j=1}^{N} G_{ij}\rho_j . \quad (3)$$

Geophysical data are always contaminated with noise, thus Eq. 3 in matrix notation is:

$$g = G\rho + e \quad (4)$$

where G is the forward operator matrix or kernel, and e is a vector representing the measurement errors.

4.2. Inversion methodology

In gravity problems, density and depth estimations are linear and nonlinear problems, respectively. Therefore, finding the Moho depth via gravity data is a nonlinear problem. In nonlinear problems, models for finding depth are classified as either homogeneous, where the density contrast in the whole area is considered constant, or heterogeneous, where the density contrast varies with space. In both cases, the subsurface can be divided into rectangular prisms.

In this paper, we assumed density as a constant in the whole model.

One method for solving nonlinear problems is forward modelling, which can also be called inverse modelling if used in a fully automated process (Blakely, 1996). As inverse modelling, we used the maximum difference reduction method (Eqs. 5 to 12), an automated iterative forward modelling method presented, for the first time, by Zhou (2013), of which a brief explanation follows.

The general rule in this method is that for each *n* interation, the depth correction, for the station with the maximum absolute gravity anomaly, is at first estimated according to Eq. 5. Consequently, the depth correction at any other station is automatically updated and is proportional to the ratio of its absolute residual gravity anomalies, which are normalised by the absolute maximum residual and, then, normalised by the density contrast. For the next iteration, new anomalies are calculated using the new depths. At this point, the algorithm, after examining the various conditions, enters the next iteration or stops.

$$\Delta z_i^{n+1} = \frac{\left|\Delta g_{obs,i} - \Delta g_{cal,i}^n\right|}{C_{max}^n} \Delta^n \tag{5}$$

where

$$\Delta^n = max\left(z_0, \frac{C_{max}^n}{C_{max}^{n-1} + C_{max}^n} \Delta^{n-1}\right) \tag{6}$$

and

$$C_{max}^n = max(|\Delta g_{obs} - \Delta g_{cal}^n|). \tag{7}$$

In the first iteration, (n = 1), we need to define C_{max}^0 and Δ^0 in Eq. 6. Since no anomaly has been calculated yet, the absolute maximum of the observed anomalies must be considered as C_{max}^0 (Eq. 8). Two choices are possible for determining Δ^0. The best initial value for Δ^0 is the one that produces a gravity anomaly profile close to the observed one. Test runs showed that Δ^0 = (0 to 7) times the thickness of the infinite slab, corresponding to the maximum absolute value of the observed gravity anomaly, is a good empirical choice (Eq. 9) (Zhou, 2013). Therefore, Δ^0 values are calculated for all coefficients from 0 to 7, then Eq. 5 is calculated, and finally, the gravity anomaly values are calculated using these thicknesses. Among these calculated anomalies, the one with the smallest difference from the observed anomaly is selected. Therefore, the coefficient that produced this anomaly is considered a selective coefficient. We may also use a value of zero for the initial Δ^0. In this way, the initial depth for all stations starts with 0. Selecting the first or second method does not affect the responses, but the first method reduces the number of iterations in the algorithm. The initial depth estimation limits the range of responses according to Eq. 9.

$$C_{max}^0 = max(|\Delta g_{obs}|) \tag{8}$$

$$\Delta^0 = (0 - 7)\frac{max(|g_{obs}|)}{2\pi G\rho}. \tag{9}$$

The conditions to be taken into consideration for algorithm convergence control should be examined next. For this, we compare the sign of ($\Delta g_{obs,i} - \Delta g_{cal,i}$) with $\Delta g_{obs,i}$ in any station. Whenever these signs are different, the corresponding depth is scaled down to a portion of the depth of the previous iteration, in accordance with Eq. 10:

$$z_i^{n+1} = S z_i^n \tag{10}$$

where:

$$S = 1 - 0.5 \frac{\left|\Delta g_{obs,i} - \Delta g_{cal,i}^n\right|}{C_{max}^n}. \tag{11}$$

If the sign does not change, the iterations continue according to:

$$z_i^{n+1} = z_i^n + \Delta z_i^n. \tag{12}$$

The algorithm execution will stop whenever the chi-square criteria (Eq. 13) are satisfied:

$$\left\| \frac{Gm - d}{\sigma} \right\|_2^2 \leq N + \sqrt{2N}, \tag{13}$$

where N is the number of data and σ is standard noise deviation.

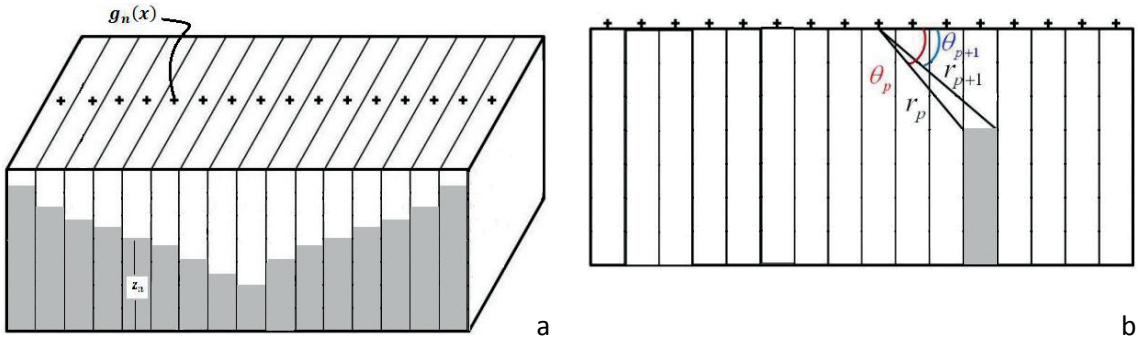

Fig. 3 - a) Underground discretisation based on 2D-rectangular blocks. The grey prisms represent the sediment layer while the white prisms correspond to the basement. b) A section of the lower surface of the gravity profile.

With regards to the algorithm convergence, it is of utmost importance to choose the proper value for z_0 in Eq. 6. A value ranging from 1 to 5 m can be a desirable choice for z_0. The z_0 value is compared with a percentage of the amount of depth correction of the previous iteration. If the correction value is smaller, the z_0 value is chosen. Also, if for large depths a too-small value is taken for z_0, the algorithm is effectively caught in a loop of infinite iterations. A small value (1 m) is selected for detecting shallow depths and a large value (5 m) for deeper ones. A flowchart of the MDR algorithm is shown in Fig. 4.

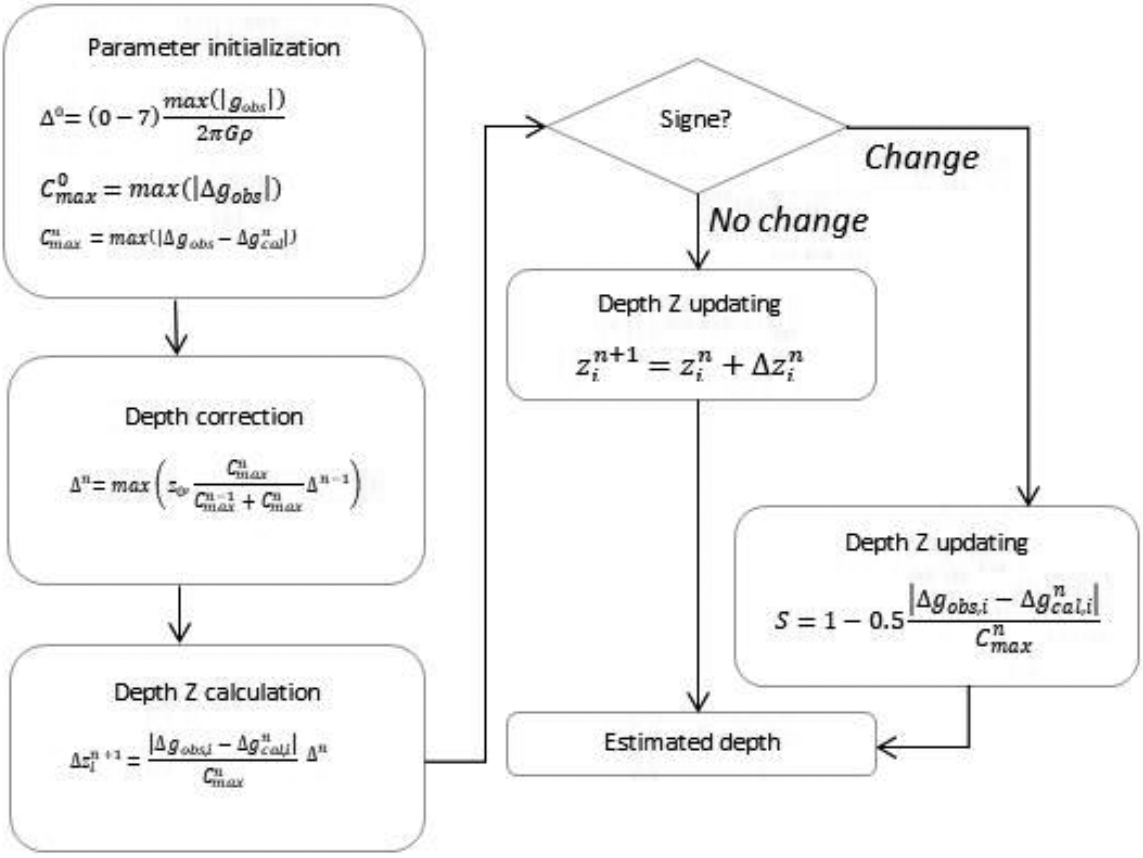

Fig. 4 - Flowchart of the MDR method.

5. Synthetic analysis

To evaluate algorithm efficiency, a model, close to the characteristics of the study area, has been considered, and three different noise levels have been applied. A profile, with a length of 252 km and 42 stations, is designed as a synthetic model. A constant density contrast of -200 kg/m^3 and depths up to 50 km are used. The shape of the underground structure is shown in Fig. 5.

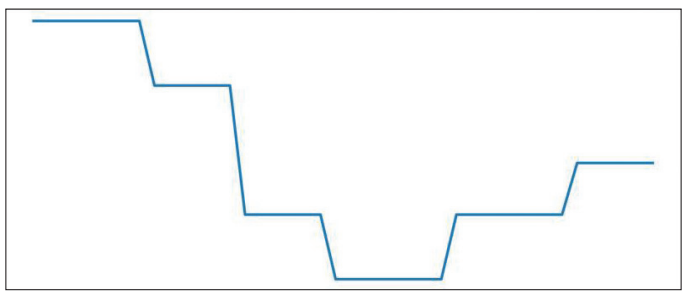

Fig. 5 - Underground structure shape of the synthetic model.

Gravity data have been calculated using Eq. 2. Since real data are always contaminated with noise, some noise is added. The common practice of adding errors to synthetic data is performed by adding random noise based upon a percentage of the datum value plus a constant (Li and Oldenburg, 1996, 1998). The latter ensures that data values close to zero do not have zero errors assigned to them. We assumed that the contaminating noise on the data is independent and Gaussian with zero means. Therefore, random numbers are generated using the randn function in Python and, then, multiplied by the expression ($\eta 1 \times g + \eta 2 \times \max|g|$). The standard noise deviation is $\eta 1 \times g$ and $\eta 2 \times \max|g|$ is the constant amount. In this paper, we considered three different noise levels: the first level being $\eta 1 = 0.01$ and $\eta 2 = 0.001$, the second level $\eta 1 = 0.02$ and $\eta 2 = 0.005$, and the third level $\eta 1 = 0.03$ and $\eta 2 = 0.01$.

Figs. 6 to 8 show simulated data and results for the inversion considering the different noise levels. For simplicity, the results of the synthetic models for all three noise levels are also shown in Table 1.

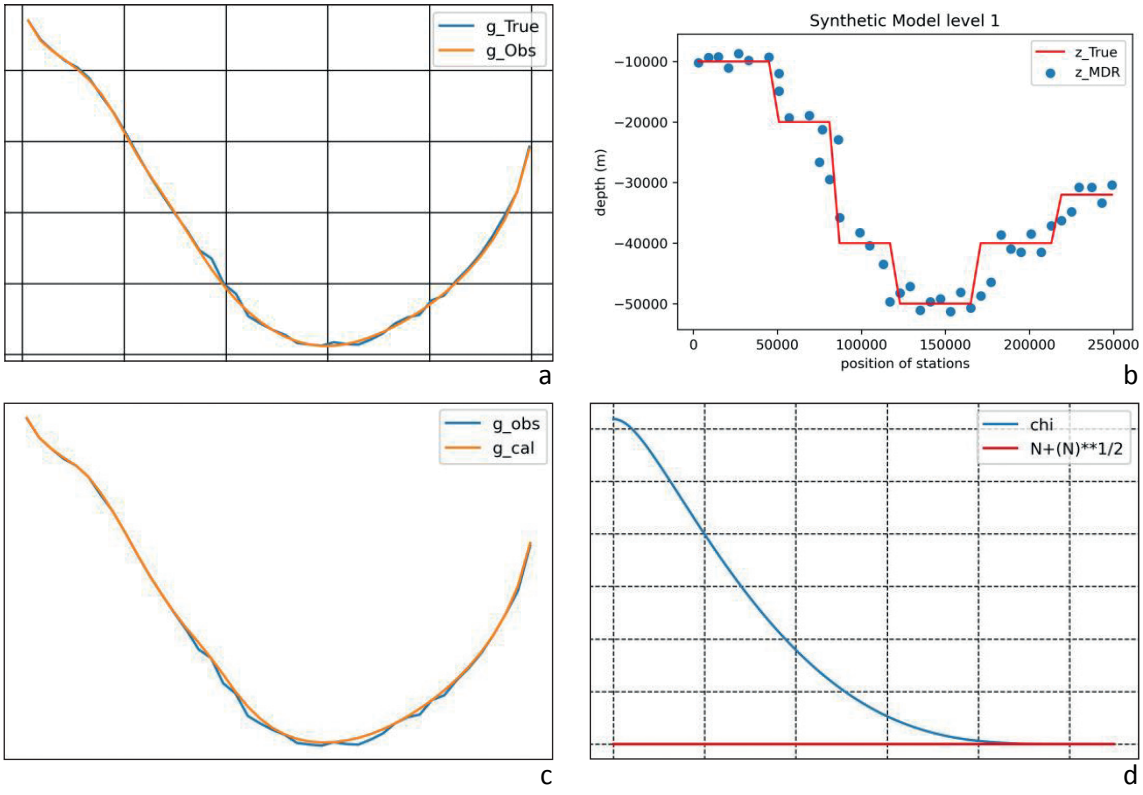

Fig. 6 - Inversion results for the synthetic model with noise level 1 ($\eta 1 = 0.01$ and $\eta 2 = 0.001$): a) true gravity and gravity with noise used as gravity observation; b) true depth (red line) and depth obtained from inversion (blue circles); c) observed (blue line) and calculated (red line) gravity; d) chi-square as function of the iteration number.

According to the results of the synthetic modelling as given in Figs. 6c to 8c, we obtained a better fit for smaller depths compared to larger ones. This is a consequence of our way of defining the noise level. This method adds further noise to larger anomalies and greater depths. Also, Table 1 shows that the maximum difference between the inverted and the original depths, in models 1 to 3, is between 3.5 and 4.5 km.

Table 1- Inversion results of the synthetic model with three different noise levels.

Model No.	Noise	Number of iterations	Data RMSE (mGal)	Model RMSE (m)	Chi-square
1A	$\eta 1 = 0.01$ $\eta 2 = 0.001$	10,495	2.5324	3,509	51.15
1B		10,804	2.4755	3,639	51.15
2	$\eta 1 = 0.02$ $\eta 2 = 0.005$	11,956	4.0043	4,304	51.16
3	$\eta 1 = 0.03$ $\eta 2 = 0.01$	12,370	5.0845	4,519	51.16

The conformity degree of calculated and observed anomalies is expressed by the root-mean-square error (RMSE), with values between 2.4 and ~5 mGal, which correspond to the magnitude of the added noise. Hence, for this synthetic model, the MDR method achieves an accurate data fit (Figs. 6b to 8b).

Model 1 was calculated twice to show the effect of initial depth selection using Bouguer slab estimation (model 1A) and zero-depth for all stations (model 1B). Although the results are remarkably similar, the number of iterations will increase in the presence of more stations or greater depths.

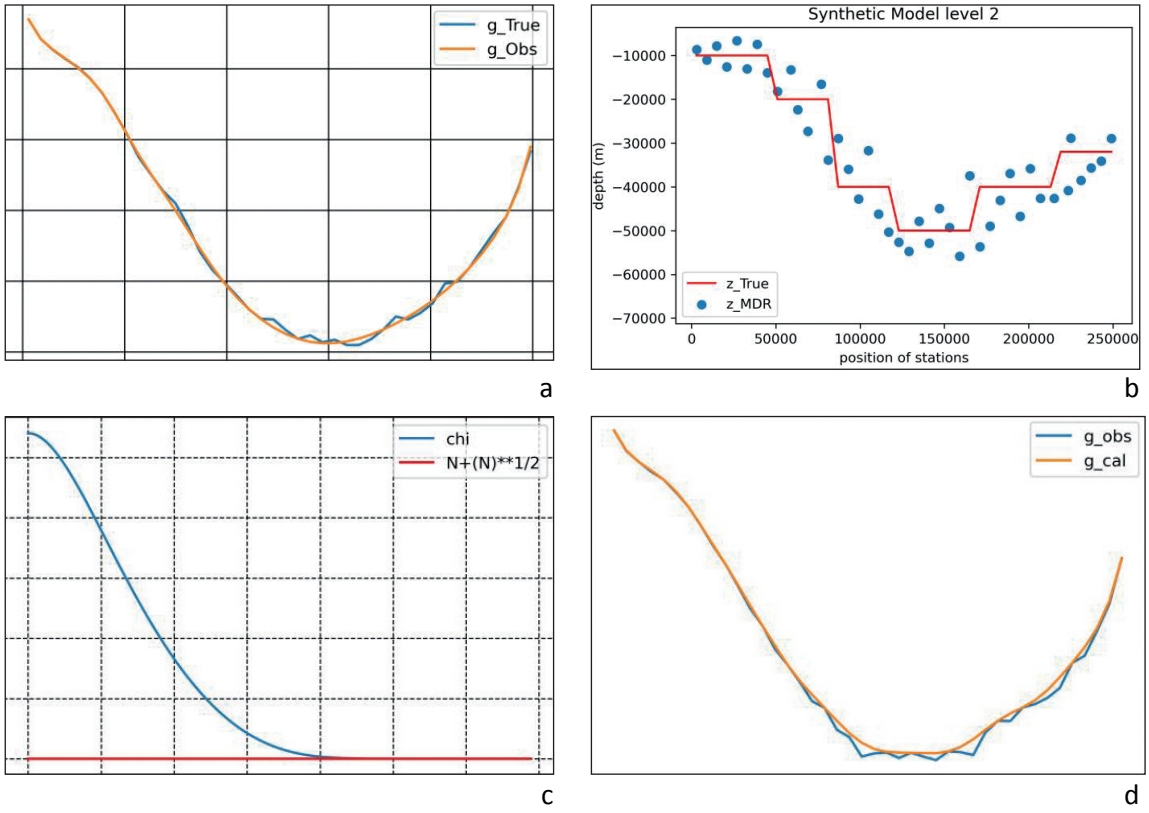

Fig. 7 - Inversion results for the synthetic model with noise level 2 ($\eta 1 = 0.02$ and $\eta 2 = 0.005$): a) true gravity and gravity with noise used as gravity observation; b) true depth (red line) and depth obtained from inversion (blue circles); c) observed (blue line) and calculated (red line) gravity; d) chi-square as function of the iteration number.

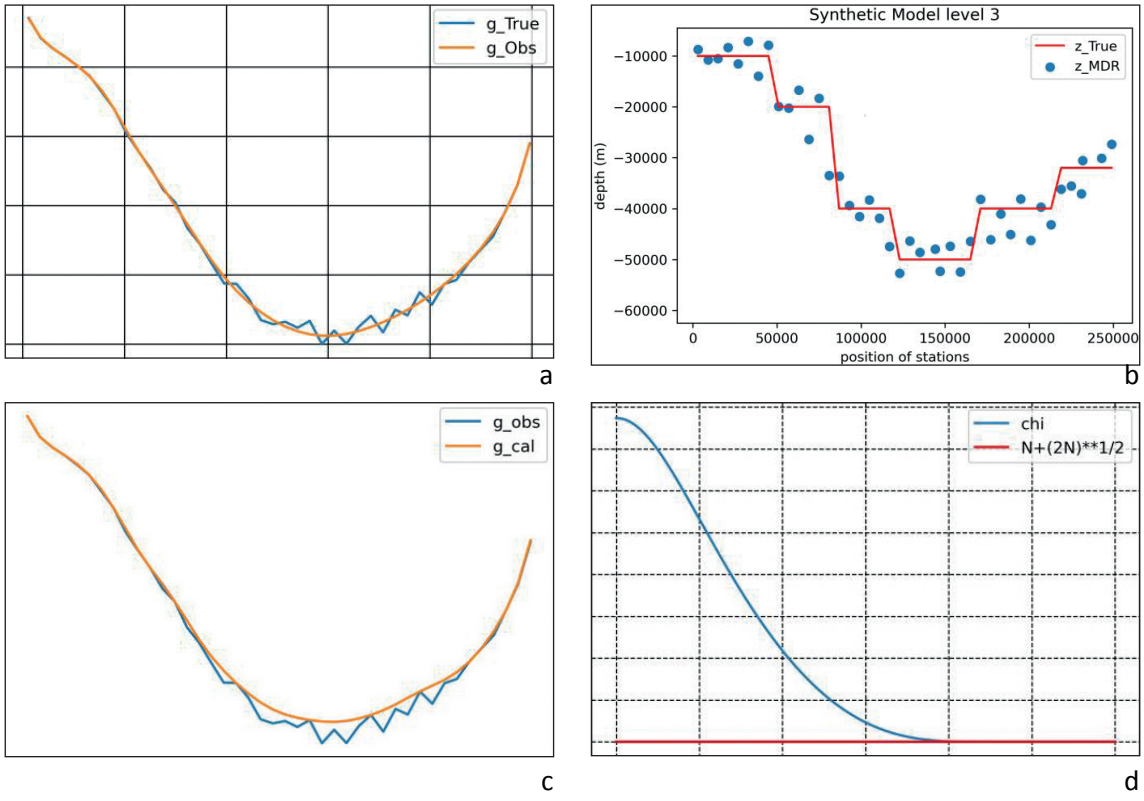

Fig. 8 - Inversion results for the synthetic model with noise level 3 ($\eta 1 = 0.03$ and $\eta 2 = 0.01$): a) true gravity and gravity with noise used as gravity observation; b) true depth (red line) and depth obtained from inversion (blue circles); c) observed (blue line) and calculated (red line) gravity; d) chi-square as function of the iteration number.

According to Table 1, the number of iterations increases with the rising noise levels.

Given that the number of data is 42, the $N + \sqrt{2}N$ value as the targeted noise level in the chi-square formula is about 51.17. According to Table 1, the algorithm stops before reaching this value for all noise levels.

6. Results and discussion

In the previous section, we examined the method with synthetic data and here we apply the method to real data. Since we used the MDR algorithm in 2D modelling, three profiles (AA', BB', and CC', see Fig. 1) were selected from the grid in the deepest area with the largest Bouguer anomalies, and where Moho depth is most controversial among researchers. These parallel profiles cross Iran in the SW-NE direction, starting from a point in the ZFTB and passing Zagros and parts of central Iran (Fig. 2). The profile length is between 460 and 480 km, and the distance between the stations is approximately 6.6 km. The profile lengths and sampling intervals are selected based on Li and Oldenburg (1996) and Boulanger and Chouteau (2001). In our algorithm, density contrast is considered constant in the study area. According to geophysical studies in this region (Mousavi and Ebbing, 2018; Ardestani and Mousavi, 2023), the best average density contrast is -100 kg/m^3.

Figs. 9 to 11 show data and inversion results. For a better assessment, the maximum Moho depth beneath the profiles in selected zones is summed up in Table 2.

Table 2 - Inversion results of three profiles in the study area.

Max Depths	ZFTB (km)	SSZ (km)	UDMA (km)	Central Iran (km)
Profile AA'	45	58	38	40
Profile BB'	45	68	39	40
Profile CC'	45	56	52	42

According to our results, along the three profiles, the maximum Moho depth is 45 km for ZFTB, followed by an abrupt deepening to up to 68 km in the SSZ, and a new thinning in the UDMA zone and central Iran, where the maximum depths are 52 and 42 km, respectively. Qualitatively, these results were expected, and are explained by varying tectonic activities and geological history in Zagros and central Iran.

In modelling, the best responses are those that fit the observed data and, at the same time, concur with the geological structures. With the RMSE factor, we can check the algorithm ability

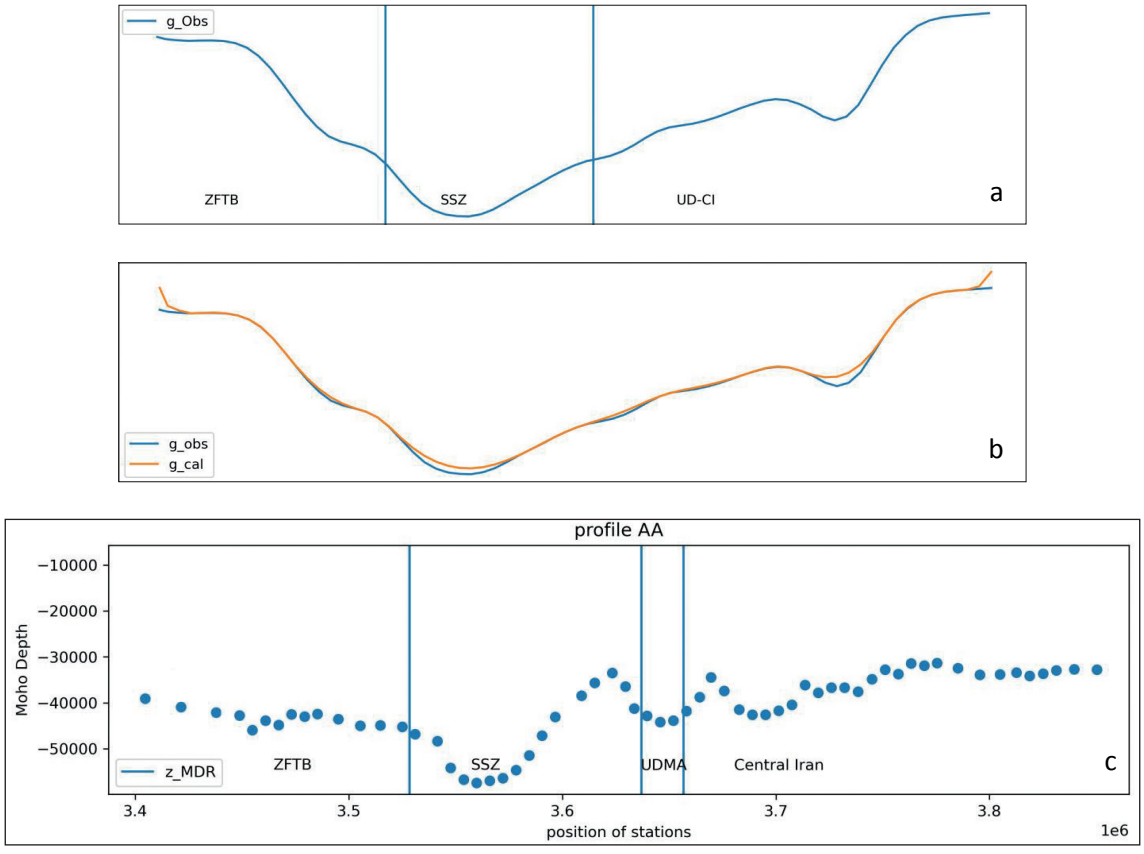

Fig. 9 - Inversion results for real data (profile AA'): a) observed gravity anomaly; b) observed gravity anomaly (blue line) and calculated gravity anomaly (red line); c) Moho depth estimation.

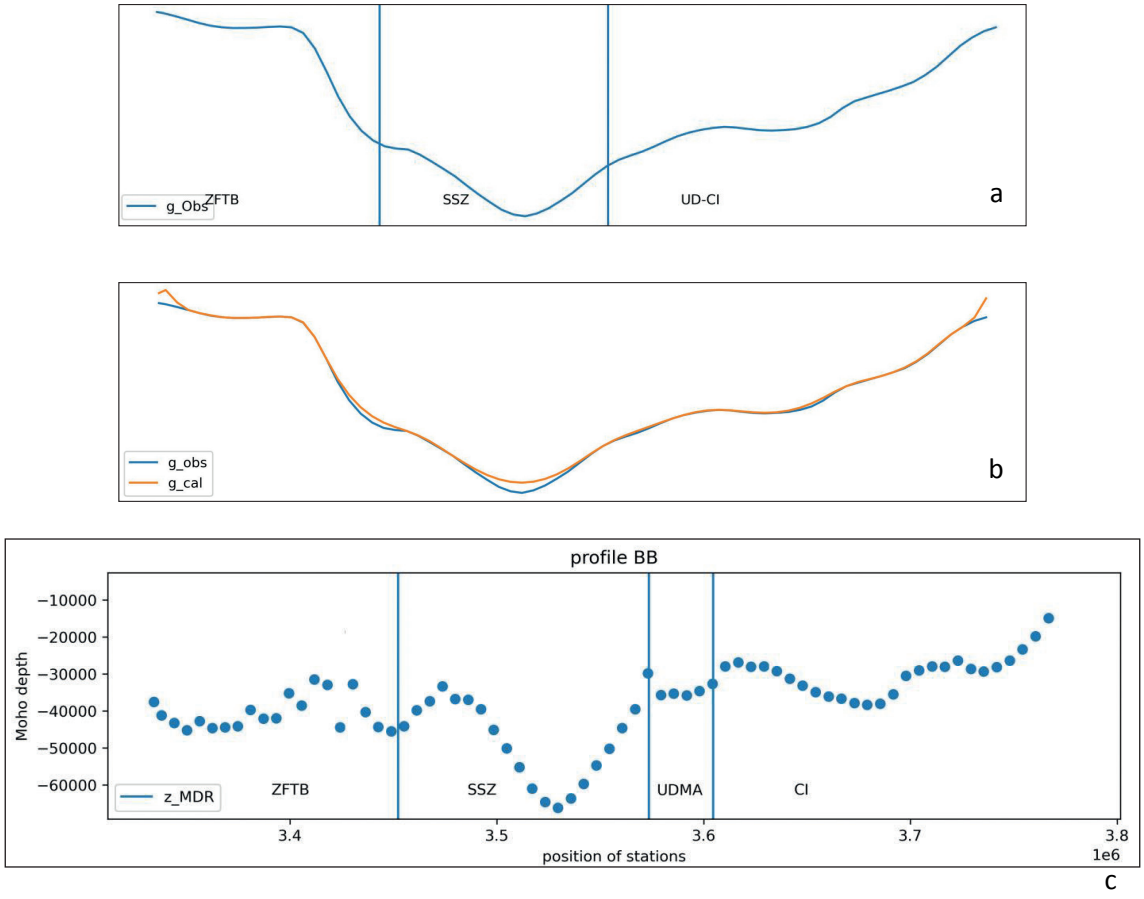

Fig. 10 - Inversion results for real data (profile BB'): a) observed gravity anomaly; b) observed gravity anomaly (blue line) and calculated gravity anomaly (red line); c) Moho depth estimation.

to find well-fitting responses. We have shown the data RMSE in Table 3, which shows that the resulting models fit the observations within their uncertainty ranges.

Table 3 - The RMSE of data misfit for the three resulting models.

	Profile AA' (mGal)	**Profile BB' (mGal)**	**Profile CC'(mGal)**
RMSE	3.2404	3.2388	3.2471

To assess the MDR algorithm's ability in underground structure reconstruction, we rely on the results of the synthetic models (as described in the previous section), and on the RMSE of the final models (Table 1). Considering that gravity data usually present level 2 noise, an average tolerance depth of 4 km, at the most, is expected in our real results. This corresponds to the results. In the second step, we compared our results with those obtained by previous researchers who used different methods. In the introduction, we explained the results of previous studies in the Zagros Mountains region. The structure of this area has been studied through the potential field and seismic methods, thus obtaining strongly varying results.

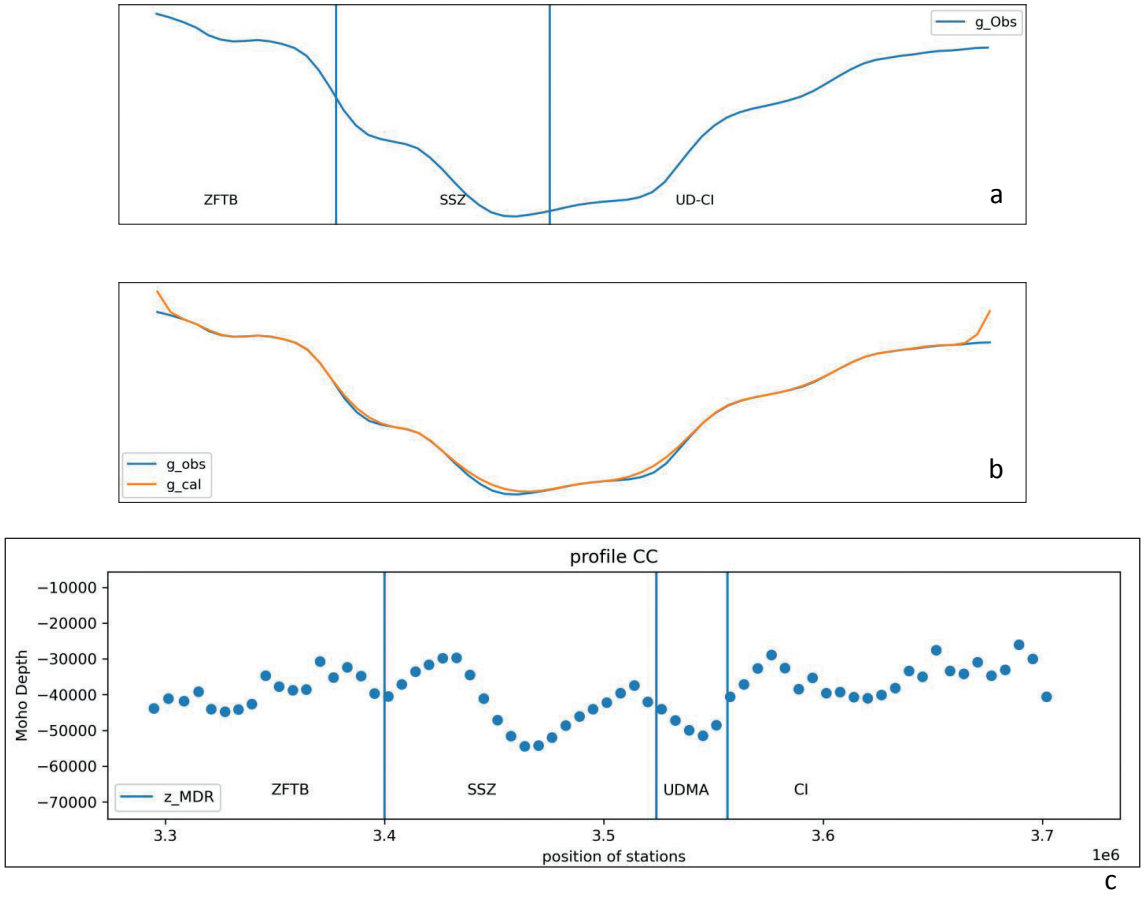

Fig. 11 - Inversion results for real data (profile CC'): a) observed gravity anomaly; b) observed gravity anomaly (blue line) and calculated gravity anomaly (red line); c) Moho depth estimation.

Our results present the same trends as those obtained in other researchers' studies. However, there are some disagreements in the details with a few. Therefore, for a better assessment, a thorough comparison is presented as follows.

First, our results are compared with the findings of Mousavi and Ebbing (2018), who applied inversion of elevation and geoid anomaly data combined with thermal analysis. The location of our AA' profile corresponds to their AA' profile. Although the two studies are in agreement on the Moho depth in the ZFTB, SSZ, and central Iran, there is disagreement with regards to such depth in the UDMA zone. The maximum Moho depth in the UDMA, in Mousavi and Ebbing's (2018) findings and in our result, is 48 and 38 km, respectively (Fig. 12a).

As an example of seismic work, we compare our results with Paul *et al*. (2006), cited the most by other researchers. Our BB' profile corresponds to their BB' profile. They acquired Moho depths of 45, ~70, and ~42 km with receiver function analysis in the ZFTB, SSZ, UDMA and central Iran, whereas our results in these areas are 48, 68, and ~39 km. Thus, the two results are remarkably similar (Fig. 12b).

Another example of seismic method is the study of Manaman and Shomali (2010). Their technique was PWI, and, in most parts of the selected profile, their results were about 40 to 45 km. However, they encountered an abrupt deepening to about 65 km in the profile centre. For these reasons, the results of our BB' profile match theirs (Fig. 12b).

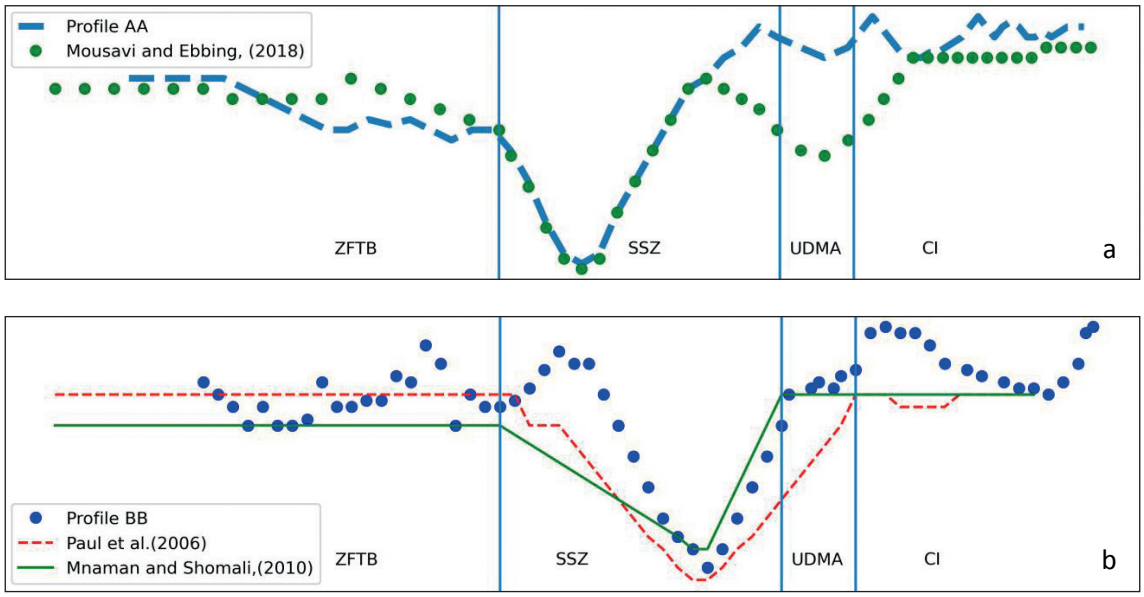

Fig. 12 - Comparison between modelling results of: a) our AA'profile with Mousavi and Ebbing (2018) and b) our BB' profile with Paul *et al*. (2006) and Manaman and Shomali (2010).

Although the MDR algorithm has previously been used by Zhou (2013) to find the thickness of shallow sedimentary basins (up to 9 km), it is an efficient method for determining depth in the Moho range (40-60 km in our study), without any changes. The only difference is that the iteration number increases in finding deeper depths.

The method can be used to determine the bedrock topography, if in the presence of denser gravity data with smaller grid-spacing (i.e. approximately 1-2 km). In this way, we can remove the Moho effect from the Bouguer anomaly, and use the residual anomalies for reconstructing the bedrock topography through the expressed method.

The technique has no limitation for upward or aero-gravity data sets. In these situations, it is necessary to correct the data to the ground level before running the model.

7. Conclusions

In this paper, two main factors have been considered simultaneously. The first is an application assessment of the MDR algorithm in the rebuilding of the subsurface structure, notably for the Moho depth, which is deeper than the typical sedimentary basin. The second is the finding of the Moho depth beneath the Zagros Mountains, which is debated but still important to know. To find the effect of gravity, we subdivided the subsurface into vertical prismatic cells, and, then, used the MDR method as a stable and automatic algorithm for 2D-inverse modelling. Iterations start from zero depth or from an initial depth model created through an infinite slab approximation of the Bouguer anomalies. Therefore, the depths are updated iteratively. The depth increase at each station is proportional to the ratio of the difference between the observed gravity and the calculated gravity, normalised to the maximum value of this difference, along the profile, at each iteration. Stabilisation is implemented by tracking the sign change of the residual gravity anomaly, at each station and each iteration, so as to force the convergence towards a single

direction. Two cases were studied: one with a synthetic data set (Figs. 6 to 8) and another with a field data set (Figs. 9 to 11). We tested the synthetic model with three different noise levels, all of which can reconstruct the real depth quite well. For the real data, the study area in central Zagros was modelled using high-resolution ground gravity data from three profiles. The results are generally in good agreement with previous studies. The algorithm has been written in Python.

Acknowledgments. The authors express their deepest gratitude to The National Cartographic Center of Iran, for sharing their data.

REFERENCES

Agar R.A.; 1987: *The Najd fault system revisited: a two-way strike-slip orogen in the Saudi Arabian shield.* J. Struct. Geol., 9, 41-48.

Alavi M.; 1994: *Tectonics of the Zagros orogenic belt of Iran: new data and interpretations*. Tectonophys., 229, 211-238.

Allen M.B., Jackson J. and Walker R.; 2004: *Late Cenozoic reorganization of the Arabia Eurasia collision and the comparison of short-term and long-term deformation rates.* Tectonics, 23, TC2008, 17 pp., doi: 10.1029/2003TC001530.

Ardestani V.E. and Mousavi N.; 2023: *The Moho relief beneath the Zagros collision zone through modeling of ground-based gravity data and utilizing open-source resources in Python*. Pure Appl. Geophys., 180, 909-918, doi: 10.1007/s00024-022-03221-7.

Barbosa V.C.F., Silva J.B.C. and Medeiros W.E.; 1997: *Gravity inversion of basement relief using approximate equality constraints on depths.* Geophys., 62, 1745-1757.

Barbosa V.C.F., Silva J.B.C. and Medeiros W.E.; 1999a: *Gravity inversion of a discontinuous relief stabilized by weighted smoothness constraints on depth*. Geophys., 64, 1429-1437.

Barbosa V.C.F., Silva J.B.C. and Medeiros W.E.; 1999b: *Stable inversion of gravity anomalies of sedimentary basins with nonsmooth basement reliefs and arbitrary density contrast variations*. Geophys., 64, 754-764.

Berberian M.; 1997: *Seismic sources of the Transcaucasian historical earthquakes*. In: Giardini D. and Balassanian S. (eds), Historical and Prehistorical Earthquakes in the Caucasus, NATO ASI Series 2, Environment-28, Kluwer Academic Publishing, Dordrecht, The Netherlands, pp. 233-311, doi: 10.1007/978-94-011-5464-2_13.

Berberian M. and King G.C.P.; 1981: *Towards a paleogeography and tectonic evolution of Iran*. Can. J. Earth Sci., 8, 210-265.

Berberian F., Muir I.D., Pankhurst R.J. and Berberian M.; 1982: *Late Cretaceous and Early Miocene Andian-type plutonic activity in northern Makran and central Iran*. J. Geol. Soc. (London, U.K.), 139, 605-614.

Blakely R.J.; 1996: *Potential theory gravity and magnetic application*. Cambridge University Press, Cambridge, UK, 461 pp., doi: 10.1017/CBO9780511549816.

Bott M.H.P.; 1960: *The use of rapid digital computing methods for direct gravity interpretation of sedimentary basins*. Geophys. J. R. Astron. Soc., 3, 63-67.

Boulanger O. and Chouteau M.; 2001: *Constraint in 3D gravity inversion*. Geophys. Prospect., 49, 265-280, doi: 10.1046/j.1365-2478.2001.00254.x.

Brown G.F. and Jackson R.O.; 1960: *The Arabian shield*. In: Proc. 21st International Geological Congress, Copenhagen, Denmark, vol. 9, pp. 69-70.

Dehghani G. and Makris J.; 1984: *The gravity field and crustal structure of Iran.* Neues Jahrb. Geol. Palaeontol. Abh., 168, 215-229.

Delaloye M., Jenny J. and Stampfli G.; 1981: *K-Ar dating in the eastern Elburz (Iran)*. Tectoniphys., 79, T27-T36.

Freeden W.; 2021: *Decorrelative Mollifier Gravimetry: basics, ideas, concepts, and examples, 1st ed.* Birkhäuser, Cham, Switzerland, 482 pp.

Guest B., Guest A. and Axen G.; 2007: *Late Tertiary tectonic evolution of northern Iran: a case for simple crustal folding*. Global Planet. Change, 58, 435-453, doi: 10.1016/j.gloplacha.2007.02.014.

Hansen P.C.; 1998: *Rank-deficient and discrete Ill-posed problems: numerical aspects of linear inversion*. SIAM, Philadelphia, PA, USA, 247 pp.

Husseini M.I.; 1988: *The Arabian Infracambrian extensional system*. Tectonophys., 148, 93-103.

Jackson D.D.; 1979: *The use of a priori data to resolve non-uniqueness in linear inversion.* Geophys. J. R. Astron. Soc., 57, 137-157.

Jackson J., Haines J. and Holt W.; 1995: *The accommodation of Arabia-Eurasia plate convergence in Iran*. J. Geophys. Res.: Solid Earth, 100, 15205-15219, doi: 10.1029/95JB01294.

Jimenez-Munt I., Fernàndez M., Saura E., Vergés J. and Garcia-Castellanos D.; 2012: *3-D lithospheric structure and regional/residual Bouguer anomalies in the Arabia-Eurasia collision (Iran)*. Geophys. J. Int., 190, 1311-1324, doi: 10.1111/j.1365-246X.2012.05580.x

Leão J.W.D., Menezes P.T.L., Beltrão J.F. and Silva J.B.C.; 1996: *Gravity inversion of basement relief constrained by the knowledge of depth at isolated points*. Geophys., 61, 1702-1714.

Li Y. and Oldenburg D.W.; 1996: *3D inversion of magnetic data.* Geophys., 61, 394-408.

Li Y. and Oldenburg D.W.; 1998: *3D inversion of gravity data.* Geophys., 63, 109-119.

Manaman N.S. and Shomali H.; 2010: *Upper mantle S-velocity structure and Moho depth variations across Zagros belt, Arabian-Eurasian plate boundary*. Phys. Earth Planet. Inter., 180, 92-103.

Manaman N.S., Shomali H. and Koyi H.; 2011: *New constraints on upper-mantle S-velocity structure and crustal thickness of the Iranian plateau using partitioned waveform inversion.* Geophys. J. Int., 184, 247-267, doi:10.1111/j.1365-246X.2010.04822.x.

Molinaro M., Leturmy P., Guezou J-C., Frizon de Lamotte D. and Eshraghi S.A.; 2005: *The structure and kinematics of the south-eastern Zagros fold-thrust belt, Iran: from thin-skinned to thick-skinned tectonics*. Tectonics, 24, TC3007, 19 pp., doi: 10.1029/2004TC001633.

Motaghi K., Tatar M., Priestley K., Romanelli F., Doglioni C. and Panza G.F.; 2015: *The deep structure of the Iranian Plateau*. Gondwana Res., 28, 407-418, doi: 10.1016/j.gr.2014.04.009.

Motavalli-Anbaran S.H., Zeyen H., Brunet M.F. and Ardestani V.E.; 2011: *Crustal and lithospheric structure of the Alborz Mountains, Iran, and surrounding areas from integrated geophysical modelling*. Tectonics, 30, TC5012, 16 pp., doi: 10.1029/2011TC002934.

Mousavi N. and Ebbing J.; 2018: *Basement characterization and crustal structure beneath the Arabia-Eurasia collision (Iran): a combined gravity and magnetic study*. Tectonophys., 731-732, 155-171, doi: 10.1016/j.tecto.2018.03.018.

Mousavi N. and Fullea J.; 2020: *3-D thermochemical structure of lithospheric mantle beneath the Iranian Plateau and surrounding areas from geophysical-petrological modelling*. Geophys. J. Inter., 222, 1295-1315.

Mouthereau F., Lacombe O. and Verges J.; 2012: *Building the Zagros collisional orogen: timing, strain distribution and the dynamics of Arabia/Eurasia plate convergence*. Tectonophys., 532, 27-60.

Oldenburg D.W.; 1974: *The inversion and interpretation of gravity anomalies*. Geophys., 39, 526-536.

Parker R.; 1973: *The rapid calculation of potential anomalies*. Geophys. J. R. Astron. Soc., 31, 447-455.

Paul A., Kaviani A., Hatzfeld D., Vergne J. and Mokhtari M.; 2006: *Seismological evidence for crustal-scale thrusting in the Zagros mountain belt (Iran)*. Geophys. J. Int., 166, 227-237, doi: 10.1111/j.1365-246X.2006.02920.x.

Paul A., Hatzfeld D., Kaviani A., Tatar M. and Péquegnat C.; 2010: *Seismic imaging of the lithospheric structure of the Zagros mountain belt (Iran)*. Geol. Soc. Spec. Publ., 330, 5-18, doi: 10.1144/SP330.2.

Pilkington M. and Crossley D.J.; 1986: *Determination of crustal interface topography from potential fields*. Geophys., 51, 1277-1284.

Snyder D.B. and Barazangi M.; 1986: *Deep crustal structure and flexure of the Arabian Plate beneath the Zagros collisional mountain belt as inferred from gravity observations*. Tectonics, 5, 361-373, doi: 10.1029/TC005i003p00361.

Tunini L., Jiménez-Munt I., Fernàndez M., Vergés J. and Villaseñor A.; 2015: *Lithospheric mantle heterogeneities beneath the Zagros Mountains and the Iranian Plateau: a petrological-geophysical study*. Geophys. J. Int., 200, 596-614, doi: 10.1093/gji/ggu418.

Vogel C.R.; 2002: *Computational methods for inverse problems*. SIAM, Philadelphia, PA, USA, 195 pp., doi: 10.1137/1.9780898717570.

Zanchi A., Zanchetta S., Berra F., Mattei M., Garzanti E., Molyneux S., Nawab A. and Sabouri J.; 2009a: *The Eo-Cimmerian (Late? Triassic) orogeny in north Iran.* Geol. Soc. Spec. Publ., 312, 31-55, doi:10.1144/SP312.3.

Zanchi A., Zanchetta S., Garzanti E., Balini M., Berra F., Mattei M. and Muttoni G.; 2009b: *The Cimmerian evolution of the Nakhlak-Anarak area, central Iran, and its bearing for the reconstruction of the history of the Eurasian margin*. Geol. Soc. Spec. Publ., 312, 261-286, doi: 10.1144/SP312.13.

Zhou X.; 2013: *Gravity inversion of 2D bedrock topography for heterogeneous sedimentary basins based on line integral and maximum difference reduction methods*. Geophys. Prospect., 61, 220-234.

Corresponding author: Mansoure Khaleghi Yalehgonbadi
Institute of Geophysics, University of Tehran
North Karegar Street, Tehran, Iran
Phone: + 98 912 400 4043; e-mail: khaleghi@ut.ac.ir, khaleghi.m90@gmail.com